Effects of Surface Orientations of Cr2O3 on CO2 Adsorption: a DFT approach

Anand Kumar, Francois Ropital, Theodorus de Bruin, Boubakar Diawara

Effects of Surface Orientations of Cr_2O_3 on CO_2 Adsorption: a DFT approach

Anand Kumar[†,‡], Francois Ropital[δ], Theodorus de Bruin[*,†] and Boubakar Diawara[‡]

[†] IFP Energies nouvelles, 1 et 4 Avenue de Bois Préau, 92852 Rueil-Malmaison, France

[‡] Chimie ParisTech, PSL Research University, CNRS, Institut de Recherche de Chimie Paris, (IRCP), F-75005 Paris, France

[δ] IFP Energies nouvelles, Rond-point de l'échangeur de Solaize, BP 3, 69360 Solaize, France

* Corresponding author: theodorus.de-bruin@ifp.fr

ABSTRACT

In the context of corrosion of stainless steel being in contact with supercritical CO_2, during the transportation step of CO_2 sequestration process, we have studied the adsorption of CO_2 molecule on different Cr_2O_3 surfaces terminations: (0001), $(01\bar{1}2)$ and $(10\bar{1}2)$ using density functional calculations. Upon CO_2 adsorption, the formation of physisorbed and chemisorbed species are found to be dependent on different surface terminations. The analyses of the optimized geometrical parameters, vibrational frequencies and atomic charges revealed the formation of a carboxylate species and a carbonate on O layer terminated-(0001), $(10\bar{1}2)$ and a carbonate species on Cr layer-$(01\bar{1}2)$ facets, respectively. The chemical bonding analysis depicts the formation of a covalent bond between the carbon and surface oxygen (O_s) atom and between the oxygen atom of the CO_2 molecule and Cr atom. Additionally, the electron density distributions (calculated from Bader's theory) show a net electron transfer from the surface to the CO_2 molecule, turning the latter into an ionic species. The calculated adsorption energies and C-O_s vibrational frequencies are in good agreement with the available experimental data and emphasize the formation of carbonates for non-(0001) surface termination.

Keywords: CO_2 adsorption, Chromium oxide surfaces, Carboxylates, Surface carbonates, Periodic DFT, DOS, Bader charge analysis, Vibrational frequency.

1. Introduction

In the present scenario, global warming is one of the foremost challenges which plagues the human species. The significantly increased atmospheric CO_2 concentrations in the last few decades have been acknowledged as a key contributor to global warming [1]. An efficient solution to avoid CO_2 emissions in the atmosphere is the process of CO_2 Capture and Storage (CCS) [2]. A key step to this process is the transportation of CO_2, from the place where it is generated to the storage site, for which stainless steel pipelines can be used. For efficiency reasons, CO_2 is transported under supercritical conditions. However, due to the presence of water and other contaminants, stainless steel may undergo corrosion [3,4]. To gain more insight in this undesired process, we need to better understand the way CO_2 interacts with the chromia passive layer that protects the underlying iron base phase from oxidation. It is an obvious statement that the composition, morphology and the surface structure determine the chemical and electronic properties occurring at the surface.

The passive layer of stainless steel is made of polycrystalline chromia whose popular facet is the polar (0001) surface [5], whereas other dominating facets are the nonpolar $(01\bar{1}2)$ and $(10\bar{1}2)$ surfaces. These different surface facets are illustrated in Fig. 1.
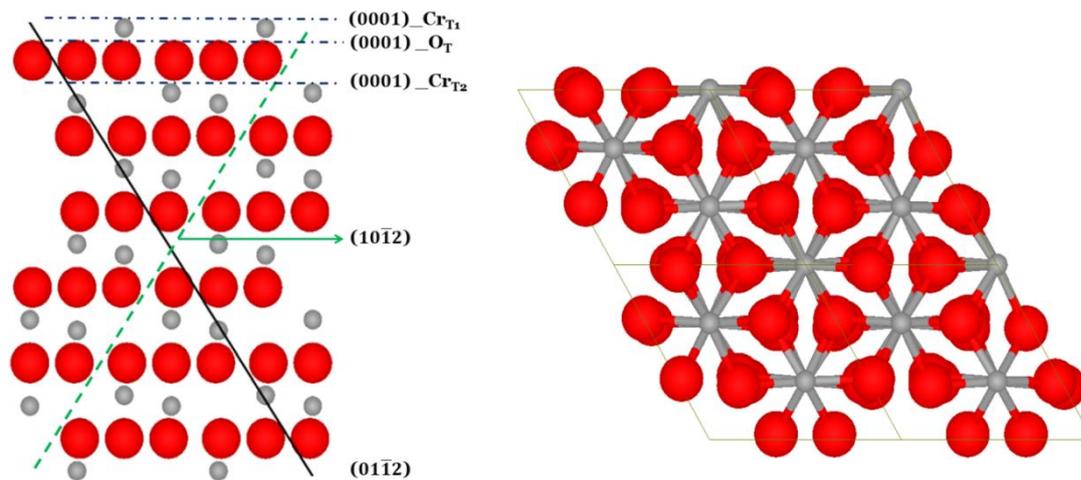

Fig. 1. Left: Three different facets (0001), $(01\bar{1}2)$, and $(10\bar{1}2)$ of chromium oxide surface; (right) top view of 2×2 cell (0001) Cr_2O_3.

.

One can observe that the $(10\bar{1}2)$ facet follows the path of minimum cleavage with the minimum surface energy before and after relaxation and hence, it is the most likely surface to be observed experimentally [6]. The oxidation rate of stainless steel on hydroxylated chromia is faster than in anhydrous conditions. Hence, the study on dry Cr_2O_3 surface will also serve as a reference to understand how chemical reactivity varies upon hydroxylation.

The interaction between CO_2 and the dry chromia surface can be considered as a Lewis acid/base reaction between the basic oxygen of CO_2 and acidic chromium, and the basic oxygen of the chromia and the acidic carbon respectively. The overall reaction can be described by Eq. 1:

$$CO_{2(gaz)} + O_{surf}^{2-} \; \rightarrow \; [CO_2\,(ads) - O_{surf}]^{\,\delta-} \; \rightarrow \; CO_3^{2-}\,(ads) \qquad\qquad (Eq.\ 1)$$

Different coordination modes of CO_2 with the oxide surface will lead to the formation of various adsorbed species comprising linear unperturbed physisorbed CO_2, bent $CO_2^{\delta-}$, monodentate and bidentate chemisorbed carbonates. For physisorption, the electronic structure of the adsorbate is only slightly perturbed with respect to the isolated molecular structure. In the present study, it has been characterized by a small adsorption energy (no strict threshold), similar geometry and vibrational frequencies with respect to the individual reactants, i.e., an isolated CO_2 and no covalent bond formation with the surface. On the other hand, chemisorption is designated to short bond distances interaction between adsorbates and the surface, large-binding energy (> 0.7 eV in present case), significant charge transfer and change in vibrational frequencies (similar to carboxylates or carbonates in present study). The existence of the aforementioned species has been comprehensively reviewed in the literature [7–10]. These adsorbates are often characterized using IR spectroscopy for the neutral carbon dioxide, surface carbonates or carboxylates and their formation is governed by the surface orientation and polarity [11]. The exploration related to CO_2 adsorption on the different facets of chromium oxide has remained a popular choice among the scientific community [5,11–13]. In an exhaustive infrared investigation of CO_2 adsorption on polar monocrystalline chromium oxide (0001), Seiferth et al. [12] have highlighted the occurrence of surface *carboxylates* or strongly adsorbed bent $CO_2^{\delta-}$. Differing to this, the bidentate coordination of *carbonates* is observed in the case of polycrystalline α-Cr_2O_3. This contrasting behavior is observed due to the non-exposure of

the (0001) facet on the given polycrystalline α-Cr_2O_3. In another investigation, non-polar microcrystalline α-Cr_2O_3 which exposes prevalently the $(10\bar{1}2)$ facet was characterized using FTIR analysis [5,13,14]. Later on, the formation of bidentate carbonates was observed upon CO_2 adsorption on α-Cr_2O_3 $(10\bar{1}2)$ [14]. From these reports, we can infer that the surface orientation and polarity play a decisive role in the way CO_2 adsorbs and reacts with the chromia surface. In these papers, the authors have not reported the clear bonding and charge transfer pathway picture. Moreover, aforementioned reports have limitations to explain these different ways of adsorption of CO_2. Hence, in our present study, we have investigated the CO_2 adsorption at three different surface orientations (0001), $(01\bar{1}2)$ and $(10\bar{1}2)$ of chromium oxide by exploiting computational methods to characterize the formation of the different adsorbed species and its rationalization. Similar theoretical studies of CO_2 adsorption on different transition metal oxide surfaces have reported the physisorbed and chemisorbed species forming 'charged bent-like' or 'carbonate-like' structure [15–17]. We thus have analyzed the adsorption energies, vibrational frequencies and charge transfers, isosurface differences and bonding of the adsorbed species to assess the nature of the adsorbed species.

2. Computational Details

The calculations have been carried out using the Perdew-Burk-Ernzerhof (PBE) functional [18], as implemented in VASP version 5.4.1 [19–21]. This functional is found to be suitable for both transition metal [22] and transition metal oxides [23]. Plane wave basis sets are used to expand the eigenstates of the electronic wavefunctions and the projector augmented waves (PAW) pseudopotentials for the implementation of the interaction between core and valence electrons [24]. Dispersion-corrected calculations are performed using Grimme's DFT-D3 methodology [25]. To account for the strong correlation between the d-electrons of the chromium, an on-site coulomb repulsion U-term is added to the DFT Hamiltonian, turning into DFT + U method [26,27]. Subsequently, this formalization impacts on the cell dimensions, band gap and, magnetic moment. Herewith, we have considered U and J parameters to be 5 eV and 1 eV respectively as reported in the literature [28,29]. The cutoff energy was set at 520 eV and the Brillouin zone is sampled with a $(6 \times 6 \times 2)$ Monkhorst-Pack [30] $\mathbf{k}$-point mesh for bulk Cr_2O_3, a $(3 \times 3 \times 1)$ $\mathbf{k}$-point mesh for the (0001) facet and a $(2 \times 3 \times 1)$ $\mathbf{k}$-point mesh for the $(01\bar{1}2)$ and $(10\bar{1}2)$

orientations. The (0001) slab corresponds to a $2 \times 2 \times 1$ supercell, while a "normal" unit cell is used for the $(01\bar{1}2)$ and $(10\bar{1}2)$ facets, because the unit cells are larger; all three cell now have a comparable number of atoms. The Quasi Newton algorithm was used to relax the geometries and the geometry was considered fully relaxed when the energy and forces were smaller than 10^{-4} eV and 0.01 eV/Å, respectively. Only the most stable configuration, out of an exhaustive test, were retained for further analyses (*vide infra*). For the antiferromagnetic behavior of Cr_2O_3, the spin polarized calculations have been performed with an initial magnetic moment value ($\pm$ 3 μ_B/ Cr atom) [29]. The spacing between the two periodic images along the direction perpendicular to the slab was set at 15 Å. The isolated CO_2 molecule was evaluated in a $12 \times 12 \times 12$ Å^3 cubic box.

The adsorption energy (E_{ads}) is calculated using the equation given below:

$$\Delta E_{ads} = E_{CO2/Cr2O3} - (E_{CO2} + E_{Cr2O3})$$

where $E_{CO2/Cr2O3}$, E_{Cr2O3}, and E_{CO2} represent the total electronic energies of the Cr_2O_3 slab with CO_2 adsorbed, the bare Cr_2O_3 slab, and the isolated CO_2 molecule, respectively. An analogous equation used to calculate the changes in the Gibbs Free adsorption energy, where furthermore holds that:

$$\Delta G_{ads} = \Delta H_{ads} - T\Delta S_{ads}$$

We assume that $\Delta H_{ads} \approx \Delta E_{ads} + \Delta E_{ZPE}$. Furthermore, we assume that upon CO_2 adsorption, the change in entropy is zero for the surface itself and that the translational and rotational contributions to the entropy become zero for the CO_2 molecule, once it is adsorbed. The translational and rotational entropy contributions of the gaz-phase CO2 molecule have been calculated with Gaussian with the PBE functional and the aug-cc-pVQZ basis set.

The vibrational entropy contributions were calculated from the partition functions that require the vibrational frequencies. The latter, as well as the IR intensities were calculated using Linear Response theory [31] as implemented in the VASP code [32].

Bader charge analyses [33] were performed by integrating the electron densities per atomic basins using a code developed by Henkelman [34]. The obtained net atomic charges have been used to quantify the charge transfer between the surface and the absorbed CO_2 molecule, as a function of its configuration [34]. The electronic properties like Density of States (DOS) and charge density differences were also evaluated to better understand the nature of chemical bonding. All considered models were built and optimized structures and frequencies were visualized using the Modelview visualization software developed by Diawara [35].

3. Results and discussion

3.1. *Bulk α-Cr$_2$O$_3$ and Bare α-Cr$_2$O$_3$ (0001), (01$\bar{1}$2) and (10$\bar{1}$2)*

Bulk α-Cr$_2$O$_3$

Bulk α-Cr$_2$O$_3$ crystal structure [Fig. 2(a)] can be depicted as hexagonal closed-packed arrangement of oxygen with Cr atoms occupying two-thirds of the octahedral sites. It is known that the antiferromagnetic spin-ordering represents the ground state structure and leads to more stable structure with respect to the ferromagnetic and the paramagnetic configurations. Thus, the spin polarized calculations were performed with the magnetic moment ($\pm$ 3 μ_B) on each individual Cr and antiferromagnetic spin-ordering (+−+−) where '+' and '−' refer to the α and β quantum spin states [36]. Initially, we have relaxed both the ion positions and the cell parameters of α-Cr$_2$O$_3$ and the optimized lattice parameters are presented in Table 1. The calculated structural parameters are in good accordance with the previous theoretical calculation and experimental data. The net atomic charges on Cr and O atoms of bulk Cr$_2$O$_3$ are +1.69 |*e*| and -1.13 |*e*| respectively.

Table 1 The calculated lattice parameters a and c (Å) for bulk Cr_2O_3

	Calculated (Present study)	Calculated [37]	Experimental [38]
a (Å)	5.10	5.07	4.95
c (Å)	13.73	13.84	13.56

Bare α-Cr_2O_3 (0001)

With respect to the overall charge neutrality, there are three possible slab terminations for the (0001) surface Fig 1.: single Cr layer terminated Cr_2O_3 (0001_Cr_{T1}), a single O layer Cr_2O_3 (0001_O_T), and a double Cr layer Cr_2O_3 (0001_Cr_{T2}). It is reported that polar single Cr-terminated can be stabilized via removal of half of chromium ions from the surface resulting into the half occupied terminating chromium [9]. This single terminated chromium layer leads to charge reduction and significant relaxation between the consecutive layers; hence, we have considered it in our present study. We undertake 1-Cr terminated slab with six Cr_2O_3 tri-layers [O, Cr, Cr] using two bottom tri-layers frozen and periodic model of the slab depicted in Fig. 2(b). This geometry is finalized after the benchmark test calculation of surface energies for different number of Cr_2O_3 atomic layers. The spacing between the two periodic images along the direction perpendicular to the slab surface was set at 15 Å keeping the two bottom tri-layers frozen. The calculated surface energy value of 2.17 J/m^2 is in good correspondence with reported value of 2.15 J/m^2 [39]. An important well-known inference can be made on comparing Fig. 2(a) and 2(b) that upon optimization, the Cr atom relaxes (blue dotted line) into the surface plane with O atoms which imparts compensation of electronic charges.

Bare Cr_2O_3 (10$\bar{1}$2)

The optimized bare Cr_2O_3 (10$\bar{1}$2) surface is presented in Fig. 2(c). The structure comprises two penta-layers of repeating atomic layers arranged as [O, Cr, O, Cr, O] or 12 Cr_2O_3 molecular units. The structure has only one termination, which is O-terminated (minimum cleavage pathway surface) and has stepwise geometry Fig. 2(d). This geometry is considered after evaluating surface energies for different number of atomic layers which comes out to be 1.66 J/m^2 and is in good agreement with experimental value of 1.70 J/m^2 [6].
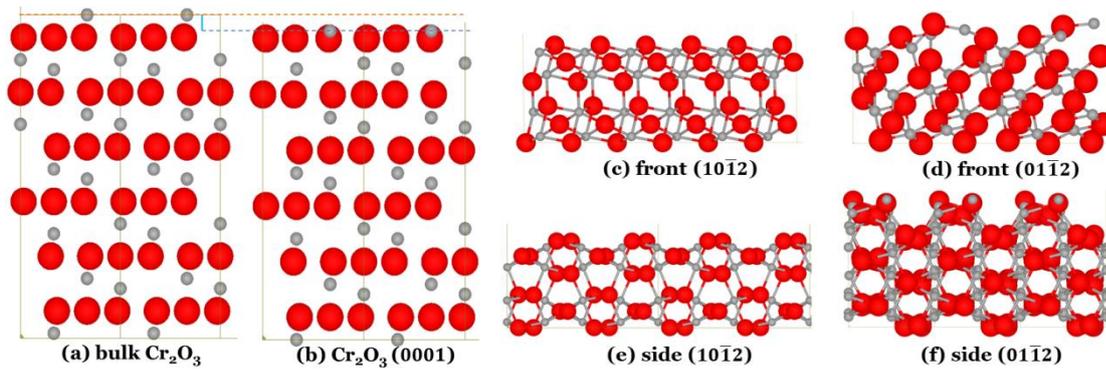
Fig. 2. (a) Bulk Cr_2O_3; (b) Cr_2O_3 (0001); (c) Cr_2O_3 (10$\bar{1}$2); (d) Cr_2O_3 (01$\bar{1}$2); side view (10$\bar{1}$2) and (f) side view (01$\bar{1}$2).

Bare Cr_2O_3 (01$\bar{1}$2)

The optimized isolated Cr_2O_3 (01$\bar{1}$2) is flat and Cr-terminated presented in Fig. 2(d). It consists of 2 penta-layers of repeating atomic layers as [O, Cr, O, Cr, O] or 24 Cr_2O_3 molecular units and exhibits surface energy value of 2.43 J/m^2.

3.2. Adsorption configurations of CO_2 on Cr_2O_3 (0001), (01$\bar{1}$2) and (10$\bar{1}$2)

Different adsorption sites for CO_2 adsorption on three different facets (0001), (01$\bar{1}$2) and (10$\bar{1}$2) of Cr_2O_3 have been explored with the coverage of 0.25 ML, which corresponds to the experimental level of adsorption [13]. Out of 4 initial adsorption structures, the most stable chemisorbed and physisorbed species (Fig. 3) are reported for each of three Cr_2O_3 facets.
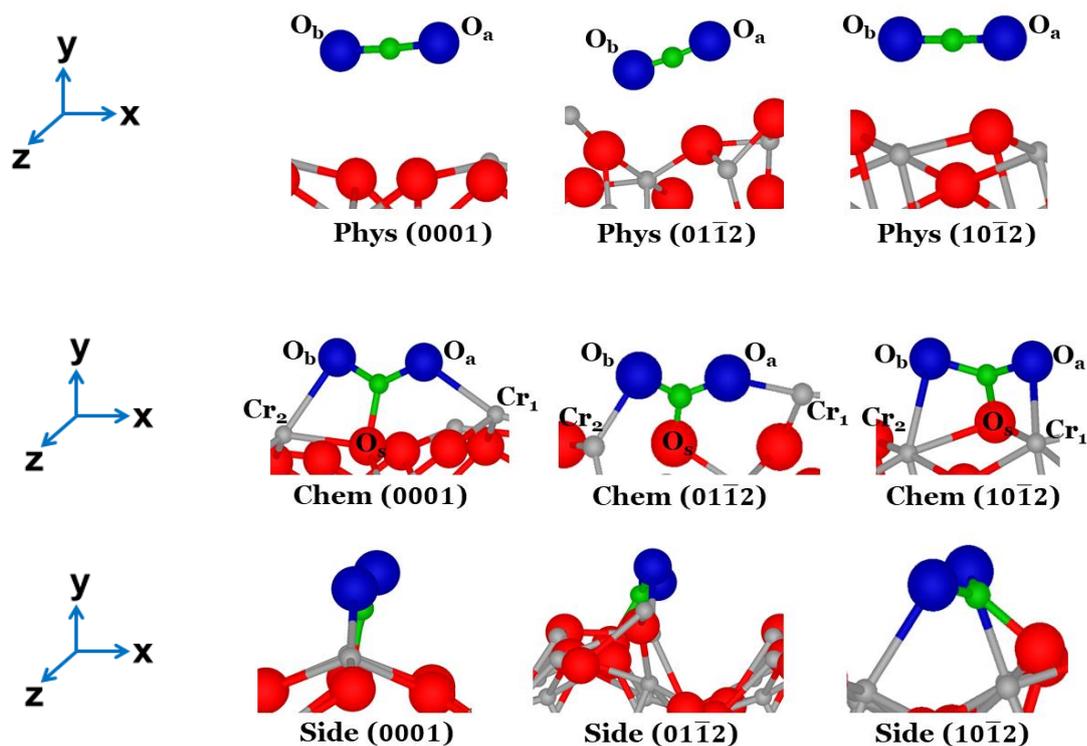
Fig. 3. Different optimized adsorption geometries of Cr_2O_3 (0001), (01$\bar{1}$2) and (10$\bar{1}$2) surface; The topmost figure represents the physisorbed structure, the middle figure represents chemisorbed species with (x-y plane) view and the figure below represents the side view (y-z plane) of the adsorbed configurations. O atoms of CO_2, C atoms, surface O atoms and Cr atoms are respectively shown in blue, green, red and dark gray.

The optimized geometrical parameters and adsorption energies (ΔE_{ads} and ΔG_{ads}) are presented in Table 2. Upon optimization, all configurations either resulted in weakly bonded (physisorbed) species or strongly bonded adsorbate species (chemisorbed). The physisorbed CO_2 molecule remains almost linear and is tilted to the surface after optimization. However, small geometrical perturbation in the bond distances (maximum 0.02 Å) and bond angles (maximum 6.19°) are observed with respect to the isolated CO_2 molecule. The C and surface O (O_s) atoms show the distance from 2.75 Å to 2.90 Å, quite larger than the normal O-C bond distances, infer to no bond formation case. In the case of chemisorption, the C atom moves down towards the surface to bond with O_s, led to the formation of bent (tridentate) CO_2 on all three surfaces. For (0001) surface, O atoms of CO_2 get bonded with the 3-fold coordinated Cr atom (Cr_{3c}), 2-fold Cr (Cr_{2c}) and 5-fold Cr (Cr_{5c}) atom for (01$\bar{1}$2) and (10$\bar{1}$2) surface and form a 'bridge-like' structure. The O-C bond distances and bond angles for chemisorbed species lies between 1.26 to 1.28 Å and

9

125.13° to 129.87° and exhibits deviations of around 0.1 Å and 50-54° with respect to an isolated linear CO_2 molecule. The C and O_s bond distances vary from 1.36 to 1.42 Å for CO_2 adsorption of different surfaces. The shortest bond length value is 1.36 Å for $(01\bar{1}2)$ surface signifies a more double bond character between O_s–C bond. Other O–C bond distances are 1.27 Å and 1.28 Å which are closer to the third bond 1.36 Å (O_s–C). Hence, for this surface $(01\bar{1}2)$, all three O–C bond distances are closer to each other and indicate the formation of a 'carbonate-like' species, whereas the bent CO_2 geometries give an indication of 'carboxylate-like' species formation on (0001) and $(10\bar{1}2)$ surfaces whose O_s–C bond distances are 1.40 Å and 1.42 Å respectively. Similar to this, Seiferth et al. [12] have experimentally verified the formation of 'carboxylate-like' species on the (0001) surface. However, unlike our results, they have mentioned the non-participation of a surface oxygen atom. We have exhaustively tried to obtain 'carboxylate-like' without involving surface oxygen, but we were unable to obtain any of such chemisorbed geometry.

Table 2.
Optimized geometrical features and adsorption energies (electronic energy and Gibbs Free energies at T=298 K) for different configurations.

Configurations	C–O$_a$ (Å)	C–O$_b$ (Å)	C–O$_s$ (Å)	Cr$_1$–O$_a$ (Å)	Cr$_2$–O$_b$ (Å)	O$_b$–C–O$_a$ (°)	ΔE$_{ads}$ (eV)	ΔG$_{ads}$ (eV)
Isolated CO$_2$	1.17	1.17				180.00		
Phys (0001)	1.17	1.17	2.89			176.43	−0.36[a]	0.2867
Phys (01$\bar{1}$2)	1.17	1.19	2.75			173.81	−0.36	0.2853
Phys (10$\bar{1}$2)	1.17	1.19	2.90			177.54	−0.59[b]	0.0521
Chem (0001)	1.26	1.27	1.40	1.98	2.04	125.13	−0.90	-0.2833
Chem (01$\bar{1}$2)	1.27	1.28	1.36	2.10	2.05	124.73	−1.26	-0.6321
Chem (10$\bar{1}$2)	1.27	1.27	1.42	2.09	2.14	129.87	−1.07[c]	-0.4559

By comparing the adsorption energy on the basis of the electronic energy and the Gibbs Free adsorption energy calculated at 298 K, one can easily see that the inclusion of the entropy has a significant impact on the energy change. For example, the physisorbed species have become unstable at 298 K, as result of their positive ΔG values, while for the chemisorbed species the ΔG values have become less negative. Since the Gibbs Free energy is a function of the temperature (and pressure), one can calculate the temperature at

which the CO_2 desorbs from the surface (for which $\Delta G=0$) to make a comparison with experiments. For example, for the (0001) surface, we calculate a desorption temperature for CO_2 of 165 K and 425 K for respectively the physisorbed and chemisorbed species, which are in very reasonable agreement with the experimental temperatures ranges of 150–250 K and 300-400 K [12] seen the approximations to calculate the entropy changes and the constant partial CO_2 pression of 1 atm. to calculate the G values.

According to our calculations, the CO_2 chemisorbed on $(01\bar{1}2)$, taking the form of a carbonate, has the highest desorption temperature and the highest adsorption energy, with respect to the chemisorption on (0001) and $(10\bar{1}2)$. This larger adsorption energy could be hypothesized that the CO_2 molecule reacts "further" and fully "integrates" in the oxide layer by becoming a carbonate species, thereby further lower the (adsorption) reaction energy and not remains limited to a carboxylate as on the (0001) and $(10\bar{1}2)$ surfaces. Summing up, we conclude from the geometrical features that a 'carbonate-like' species is formed at $(01\bar{1}2)$; such a formation would corroborate with a higher adsorption energy, whereas the bent CO_2 geometries are marked to be 'carboxylate-like' species formation with lower adsorption energies. Furthermore, it is noticed that the Cr-terminated surface leads to the formation of 'carbonate-like' species, while the O-terminated to 'carboxylate-like' species.

We have considered the increasing CO_2 coverage Θ of 1/4 ML, 1/2 ML, 1 corresponding to the ratio of CO_2 to surface Cr-atoms. Experimentally, the coverage (Θ) for an adsorption calculation is reported to be ~0.3 monolayer (ML) and hence, we have considered in our calculations a coverage Θ = 1/4 ML. However, we have also performed additional calculations with Θ = 1 ML to investigate the influence of the coverage on adsorption energy for (0001) surface (Fig. 4). The Eads for coverage Θ = 1/4 ML is –0.90 eV and for coverage Θ = 1/2 ML is –0.50 eV per CO_2 molecule. This reveals that adsorption energy decreases with increase in coverage which is consistent with experimental finding at coverage of $\Theta \sim$ 0.3 ML.

We have also explored the possibilities of bidentate and monodentate, chemisorbed species on different surfaces. Among these, we found one bidentate chemisorbed species with E_{ads} = –0.69 eV on Cr_2O_3 $(10\bar{1}2)$ surface.
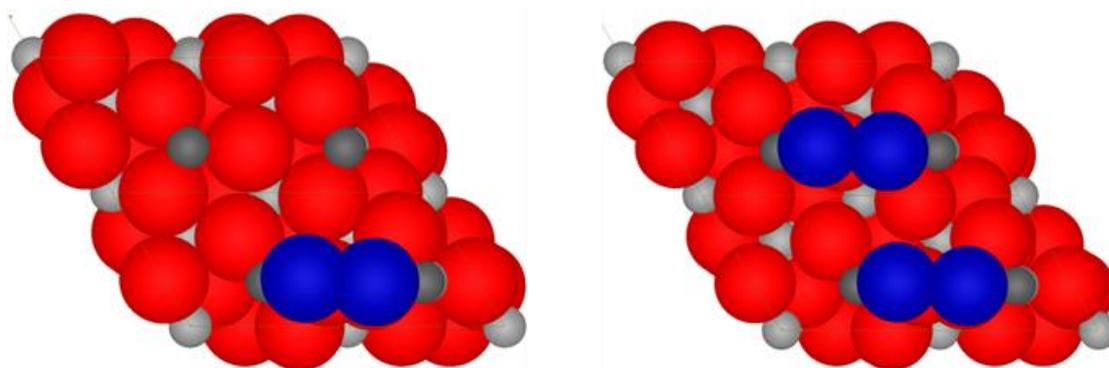
Fig. 4. CO_2 coverage Θ on (0001) Cr_2O_3 surface calculated per surface-Cr atom (indicated in dark grey): left 25%; right 50%.

3.3.   Vibrational Frequency Analyses

The harmonic vibrational frequencies were computed for the CO_2 molecule for the most stable configuration. Furthermore, the frequency evaluation yields insights in the formation of the adsorbed species. In the case of physisorption, the vibration frequencies of CO_2 molecule are nearly identical to the frequencies of the isolated CO_2 molecule, while in the chemisorbed CO_2 molecule, the frequencies shift significantly. Different vibrational modes (Fig. 5) of isolated, physisorbed and chemisorbed CO_2 molecule on different Cr_2O_3 surfaces are presented in Table 3.

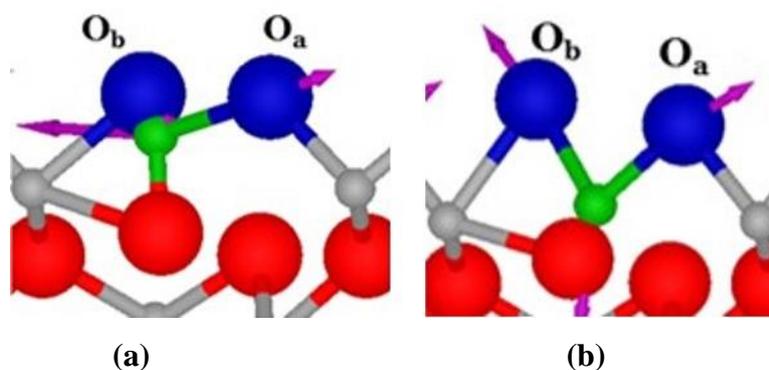**(a)**   **(b)**

Fig. 5. Different vibrational modes of CO_2 molecule; (a) Asymmetric stretching, (b) Symmetric stretching frequency

The IR frequencies and their corresponding intensities were calculated for both the physisorbed and chemisorbed species separately. Next, we merged the two spectra (each contributing 50%) into one spectrum, because the experimental spectrum simultaneously shows the frequencies of both the physisorbed and chemisorbed species. The intensities have been rescaled with respect to the most intense peak. These calculated spectra at 0 K

will be compared to the experimental ones, recorded at the lowest temperature, i.e. at 90 K for the Cr_2O_3 (0001)/Cr(110) system [12] and 100 K for the polycrystalline [12].

For the (0001) surface, the surface selection rule applies for the experimental IR spectrum as the oxide is grown on a metallic substrate (Cr_2O_3 (0001)/Cr(110) system). However, our IR calculations are made on the (0001) Cr_2O_3 slab without metallic substrate and so the surface selection rule does not apply. Accordingly, we have manually removed those frequencies that are forbidden by the surface selection rule, which states that the vibrational stretching modes that are parallel to the surface, are not observed.

In the calculated IR spectrum for the (0001) surface, the most intense peak at 2352 cm^{-1} is associated with the asymmetric stretching mode of the physisorbed CO_2: note that the symmetric stretching mode is of course IR-inactive. The less intense peak at 1245 cm^{-1} corresponds to the symmetric stretching of the (chemisorbed) carboxylate species. However, the antisymmetric peak calculated at 1660 cm^{-1} remains absent in the experimental IR spectrum, due to the parallel alignment of the O–O axis to the surface and is therefore forbidden by the surface selection rule. Furthermore, the peak observed in the experimental spectrum at 998 cm^{-1}, is not observed in the theoretical spectrum, since in our calculations chromyl groups are absent. The calculated and the experimental spectra have been superimposed and from Figure 6(a) it seen that there is a very good accordance.

In the IR spectrum for the $(01\bar{1}2)$ facet the asymmetric stretching frequency is recorded at 2371 cm^{-1} for the physisorbed CO_2. However, this spectrum is characterized by its most intensive peak at 1557 cm^{-1} attributed to the antisymmetric stretching mode of the carbonate and followed by the symmetric stretching modes at 1287 cm^{-1} and 780 cm^{-1}. The calculated IR spectrum is in good agreement with the experimental recorded spectrum as can be seen from Figure 6(b). The contrasting difference between the IR spectrum of (0001) and $(01\bar{1}2)$ is related to the presence of the antisymmetric stretching band in $(01\bar{1}2)$ and secondly a weaker signal at 1010 cm^{-1}, the latter being a key aspect to the surface carbonate formation.

We conclude that our calculations truthfully reproduce both the IR frequencies and intensities of the experimental spectra and that we can rightly attribute the nature of each vibrational modes to its experimentally recorded resonance.
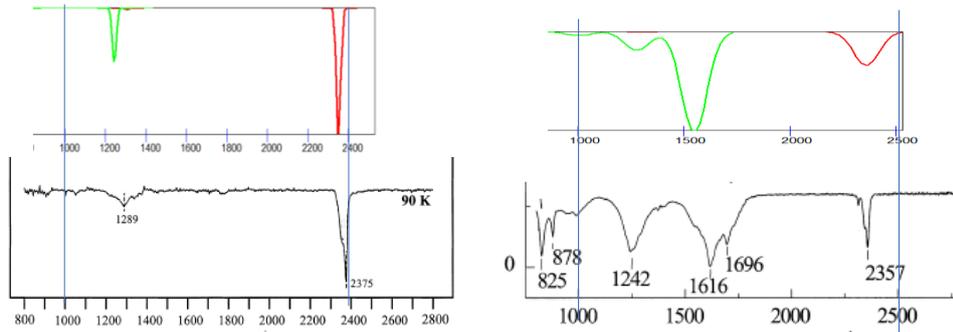
Fig. 6. Calculated (above) and experimental (below) [12] IR spectrum of CO_2 on (a) the (0001) versus Cr_2O_3 (0001)/Cr(110) and (b) the $(01\bar{1}2)$ facet versus polycrystalline. The green resonances correspond to the stretching modes of the chemisorbed CO_2 and the red one of the physisorbed CO_2. Energy in cm^{-1}.

Table 3

Vibrational frequencies (cm^{-1}) of isolated, physisorbed and chemisorbed CO2 molecule. The values in parentheses provide the experimental frequencies [12].

Configurations	Asymmetric (υ_{as})	Symmetric (υ_s)	Bending (δ)	$C–O_s$
Isolated CO_2	2365 (2349)	1317 (1333)	632 (667)	
Phys (0001)	2351 (2375)*	1310 (1301)#	614	
Phys $(01\bar{1}2)$	2361 (2349)	1308 (1333)	596	
Phys $(10\bar{1}2)$	2337 (2349)	1298 (1333)	619 (667)	
Chem (0001)	1660	1244 (1280 – 1340)	737 (744 – 840)	799
Chem $(01\bar{1}2)$	1550 (1530 – 1634)	1279	769	1003 (1050)
Chem $(10\bar{1}2)$	1606 (1530 – 1620)	1215 (1250 – 1270)	686	834

* At T=120 K temperature; # At T=150 K temperature

3.4. Charge Transfer Analyses

To understand the atomic charge distribution, we have performed Bader analysis [33,34]. Table 4 provides the Bader atomic charges on isolated, physisorbed and chemisorbed CO_2 for different Cr_2O_3 surfaces. The total electrostatic charges on isolated CO_2 molecule is calculated to be –0.01 $|e|$. From Bader charges analysis, we observe a minor charge transfer (max –0.05 $|e|$) for physisorbed CO_2 implying. For the chemisorbed species, the maximum net electron charge transfer to the CO_2 molecule is 0.33 $|e|$ at the Cr_2O_3 $(01\bar{1}2)$ surface, followed by 0.24 $|e|$ at Cr_2O_3 $(10\bar{1}2)$ surface and the smallest value of 0.11 $|e|$ at the Cr_2O_3 (0001) surface. The CO_2 molecule thus becomes each time enriched in electron

14

density and could be considered as a Lewis acid. This charge transfer causes the linear CO_2 molecule to adopt a bent geometry to stabilize the negative charge. We have also analyzed the possibility of the formation of 'carbonate-like' species (CO_3^{2-}) for all three surfaces. The overall charge value of (CO_3^{2-}) for (0001) and $(10\bar{1}2)$ are -1.26 $|e|$ and -1.34 $|e|$ but for $(01\bar{1}2)$ it is -1.61 $|e|$ which significantly resemblances the 'carbonate-like' species with a formal -2 $|e|$ charge.

Table 4 The net atomic charges ($|e|$) of isolated and adsorbed CO_2 molecule.

Configurations	O_a	O_b	C	O_s	Variation charge	CO_3^{2-}
Isolated CO_2	–0.82	–0.83	1.64		–0.01	
Phys (0001)	–1.07	–1.09	2.16		0.00	
Phys $(01\bar{1}2)$	–0.89	–0.98	1.82		–0.05	
Phys $(10\bar{1}2)$	–1.05	–1.08	2.17		0.04	
Chem (0001)	–1.14	–1.13	2.15	–1.14	–0.12	–1.26
Chem $(01\bar{1}2)$	–0.96	–0.97	1.60	–1.12	–0.33	–1.61
Chem $(10\bar{1}2)$	–1.17	–1.15	2.08	–1.10	–0.24	–1.34

To qualify the charge transfer from the surface to the molecules, we have plotted the charge density difference (CDD) :

$$\Delta\rho(r) = \rho_{Cr2O3/CO2}(r) - \rho_{Cr2O3}(r) - \rho_{CO2}(r)$$

between adsorbed configuration (Cr_2O_3/CO_2), isolated surface (Cr_2O_3) and CO_2 molecule for different isosurfaces (Figure 7). A positive value ($\Delta\rho(r) > 0$) corresponds to an accumulation of charge densities around O atoms of the CO_2 molecule (Fig. 7a) and ($\Delta\rho(r) < 0$) corresponds to loss of charge density around surface the Cr atom (Fig. 7b). From this analysis, it is found that there is a charge transfer from the surface Cr atoms to the CO_2 molecule and further due to electronegative difference between C and O atoms; electrons are distributed from the C atom to the O atoms of the CO_2 molecule. The Cr atom is bonded to four O atoms in the surface instead of six O atoms in the bulk. Due to this, Cr atoms have an excess electron density, which they lose to the CO_2 molecule upon adsorption, thus leading to a net electron density transfer from surface to CO_2 molecule.

This charge transfer from Cr atoms to adsorbate is also favored due to the selection of Cr terminated chromium oxide surface. In this case, the interaction between the adsorbates and the substrate occur via exposed chromium ions. Therefore, for Cr terminated $(01\bar{1}2)$ surface, there will be greater electron transfer as observed which led to the formation of 'carbonate-like' structure (more charged spcies) whereas for remaining two surfaces (oxygen terminated), there is 'carboxylate-like' species formation due to lesser electron transfer. Similar results have been formalized by Seiferth et al. [13]. Moreover, only the top layer of the surface participates in the electron transfer, whereas, no contribution from the subsurface layer is noted. From Bader charge analysis, we understand about the formation of carboxylates or carbonates depending upon different surface termination and isosurface analysis helps us to devise the electron charge transfer pathway, i.e., charge transfer in chemisorbed species are occurring via the Cr atom of the surface to the CO_2 molecule.
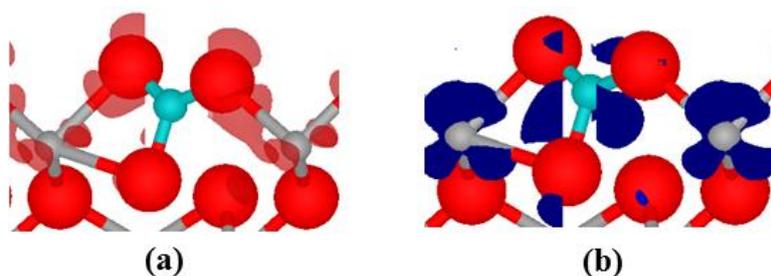

Fig. 7. Charge density difference (CDD) plot for (0001) Cr_2O_3 surface (a) positive (in red) and (b) negative for the chemisorbed configuration (in blue). The isosurfaces were plotted at ± 0.06 e/ Å^3.

3.5. Density of States

To understand the nature of chemical bonding between CO_2 molecule and different chromia surfaces, we have performed projected density of states (PDOS) calculation for the most stable geometries. PDOS is computed with high-level precision *k*-mesh of $12 \times 12 \times 1$ (for Cr_2O_3 (0001) and $4 \times 6 \times 1$ for $(01\bar{1}2)$ and (10T2) orientation). All PDOS plots are in reference to the Fermi energy, E_f. The PDOS plots for the carbon and the surface oxygen are depicted in Fig. 8. From the DOS plot, we have identified the orbital contribution of different atoms in bond formation. The bond formation between C and surface O atoms can be clearly observed by the significant overlap of their p-orbitals.
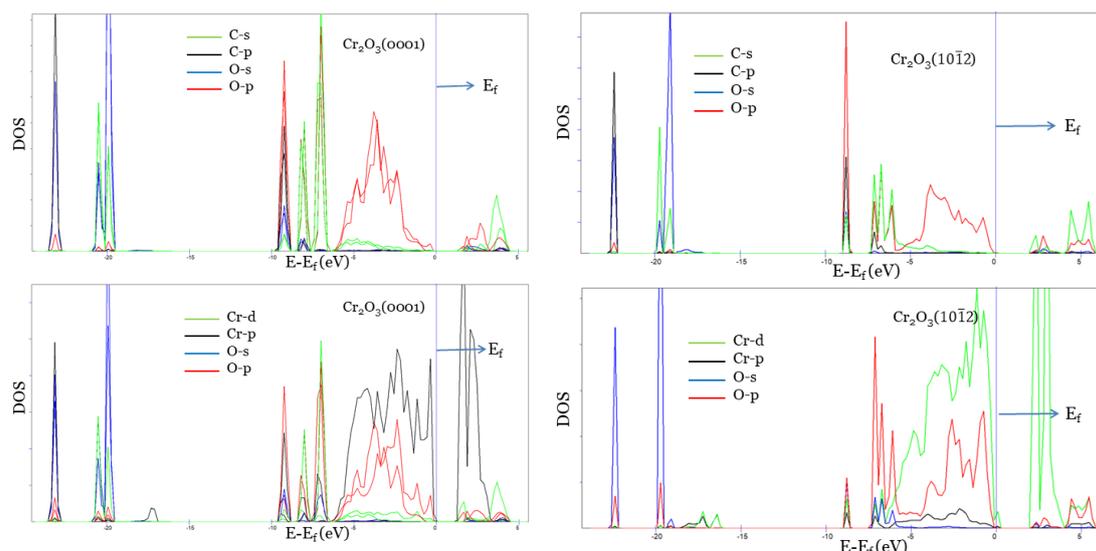
Fig. 8. PDOS plots for Cr_2O_3 (0001) and ($10\bar{1}2$) surfaces. All plots are aligned at the Fermi level.

We have also plotted the PDOS of the Cr and O atoms of CO_2. In all systems, the overlap between d-orbital of Cr and p-orbital of O atom is clearly identified. The p-orbital of Cr and s-orbital of O atoms have also contributed to the formation of Cr-O bond. The s-states of C and O atoms are also involved in bond formation.

4. Conclusions

The CO_2 adsorption on anhydrous chromia surfaces has been investigated using DFT methods. Two chromia surfaces (0001) and ($01\bar{1}2$) have a flat orientation whereas ($10\bar{1}2$) has a stepped structure. After relaxation of the geometry, the CO_2 molecule can either be physisorbed or chemisorbed. Similar to the isolated CO_2 molecule, the physisorbed CO_2 conserves its linear structure whereas the chemisorbed CO_2 converges to a 'bent-like' structure, revealing a significant geometrical deviation. The C-O_s shorter bond length indicates a more double bond character for the ($01\bar{1}2$) surface and the closer all O-C bond distance indicates a 'carbonate-like' species formation which is endorsed by greater E_{ads} value of -1.26 eV. The chemisorbed configurations for all three surfaces exhibit higher E_{ads} [-1.07 eV for ($10\bar{1}2$) surfaces and this value is in good agreement with the experimental values (-1.08 eV) [13]. The vibrational frequencies for Cr_2O_3 (0001) and ($10\bar{1}2$) are in correspondence with experimental carboxylates frequencies [12]. An extra C=O stretching frequency observed for Cr_2O_3 ($01\bar{1}2$) suggests the formation of surface carbonates. The Bader charge analysis reveals an electron charge transfer from the surface

to the CO_2 molecule. For the chemisorbed Cr_2O_3 (0001) configuration, the small (–0.11 |e|) charge transfer and 'bent-like' chemisorbed CO_2 makes it a prototype of a carboxylate ion whereas, more electron (–0.33 |e|) transfer is observed in the Cr_2O_3 (01$\bar{1}$2) case. Also, the analysis for carbonate formation shows the net charge of –1.61 |e| validate the 'carbonate-like' species formation. The charge transfer from chromium surface to the CO_2 molecule has to occur via exposed chromium atoms. Therefore, it will be greater in Cr terminated surface and thus it led to the formation of 'carbonate-like' species on (01$\bar{1}$2) whereas 'carboxylate-like' species on O terminated surfaces. From the DOS analysis, we have understood the contribution of different atomic orbitals in the Cr-O and O-C bond formation upon chemisorption.

The clarity of the adsorbed species formation will be illuminating to understand the effects of presence of water and other contaminants and then to take preventive measures against the pipeline corrosion. Also, it can be instrumental to explore the catalytic uses of chromia surface CO_2 reduction to fuels [36].

References:

[1]   U.S. Environmental Protection Agency Report. Inventory of U.S. Greenhouse Gas Emissions and Sinks: 1990-2017 (2019).

[2]   M. B. Handford, Matthew E., J. C. Abanades, E. J. Anthony, M. J. Blunt, S. Brandani, N. M. Dowell, J. R. Fernández, M. C. Ferrari, R. Gross, J. P. Hallett, R. S. Haszeldine, P. Heptonstall, A. Lyngfelt, Z. Makuch, E. Mangano, R. T. J. Porter, M. Pourkashanian, G. T. Rochelle, N. Shah, J. G. Yao, P.S. Fennell, Carbon capture and storage update, Energy Environ. Sci. 7 (2014) 130–189.

[3]   Y. Zhang, K. Gao, G. Schmitt, R.H. Hausler, Modeling steel corrosion under supercritical CO_2 conditions, Mater. Corros. 64 (2013) 478–485.

[4]   Y. Zhang, K. Gao, G. Schmitt, in: NACE International, 2011, p. 15.

[5]   H. Kuhlenbeck, C. Xu, B. Dillmann, M. Haßel, B. Adam, D. Ehrlich, S. Wohlrab, H.J Freund, U.A. Ditzinger, H. Neddermeyer, M. Neuber, and M. Neumann, Adsorption and Reaction on Oxide Surface: CO and CO_2 on Cr_2O_3(111), Ber. Bunsenges. Phys. Chem. 96 (1992) 15–27.

[6]   P.J. Lawrence, S.C. Parker, P.W. Tasker, Computer Simulation Studies of Perfect and Defective Surfaces in Cr_2O_3, J. Am. Ceram. Soc. 71 (1988) C389-C391.

[7]   U. Burghaus, Surface chemistry of CO_2 – Adsorption of carbon dioxide on clean surfaces at ultrahigh vacuum, Prog. Surf. Sci. 89 (2014) 161–217.

[8]   U. Burghaus, Surface science perspective of carbon dioxide chemistry—Adsorption kinetics and dynamics of CO_2 on selected model surfaces, Catal. Today 148 (2009) 212–220.

[9] J.A. Mejias, V. Staemmler, H.-J. Freund, Electronic states of the Cr_2O_3 (0001) surface from ab initio embedded cluster calculations, J. Phys. Condens. Matter 11 (1999) 7881–7891.

[10] H.J. Freund, M.W. Roberts, Surface chemistry of carbon dioxide, Surf. Sci. Rep. 25 (1996) 225–273.

[11] A. Zecchina, S. Coluccia, E. Guglielminotti, G. Ghiotti, Infrared study of surface properties of alpha-chromia. III. Adsorption of carbon dioxide, J. Phys. Chem. 75 (1971) 2790–2798.

[12] O. Seiferth, K. Wolter, B. Dillmann, G. Klivenyi, H.-J. Freund, D. Scarano, A. Zecchina, IR investigations of CO_2 adsorption on chromia surfaces: Cr_2O_3 (0001)/Cr(110) versus polycrystalline α-Cr_2O_3, Surf. Sci. 421 (1999) 176–190.

[13] M.W. Abee, S.C. York, D.F. Cox, CO_2 Adsorption on α-Cr_2O_3 (10$\bar{1}$2) Surfaces, J. Phys. Chem. B 105 (2001) 7755–7761.

[14] D. Scarano, G. Spoto, S. Bordiga, G. Ricchiardi, A. Zecchina, Revisiting the α-Cr_2O_3/CO interaction: an FTIR and HRTEM study 64 (1993) 307–313.

[15] A.K. Mishra, A. Roldan, N.H. de Leeuw, CuO Surfaces and CO_2 Activation: A Dispersion-Corrected DFT+U Study, J. Phys. Chem. C 120 (2016) 2198–2214.

[16] Y. Pan, C-J Liu, Q. Ge, Adsorption and protonation of CO_2 on partially hydroxylated γ-Al_2O_3 surfaces: a density functional theory study, Langmuir 24 (2008) 12410–12419.

[17] L.I. Bendavid, A.E. Carter, CO_2 Adsorption on Cu_2O(111): a DFT+U and DFT-D study, J. Phys. Chem. C 117 (2013) 26048–26059.

[18] J.P. Perdew, K. Burke, M. Ernzerhof, Generalized gradient approximation made simple, Phys. Rev. Lett. 77 (1996) 3865–3868.

[19] G. Kresse, J. Furthmüller, Efficiency of ab-initio total energy calculations for metals and semiconductors using a plane-wave basis set, Comput. Mater. Sci. 6 (1996) 15–50.

[20] G. Kresse, J. Hafner, Ab initio molecular-dynamics simulation of the liquid-metal-amorphous-semiconductor transition in germanium, Phys. Rev. B 49 (1994) 14251–14269.

[21] G. Kresse, D. Joubert, From ultrasoft pseudopotentials to the projector augmented-wave method, Phys. Rev. B 59 (1999) 1758–1775.

[22] P. Janthon, S. Luo, M. S. Kozlov, F. Viñes, J. Limtrakul, D. G. Truhlar., F. Illas:, Bulk Properties of Transition Metals: A Challenge for the Design of Universal Density Functionals, J. Chem. Theory Comput. 10 (2014) 3832–3839.

[23] J. Yan, J.K. Nørskov, Calculated formation and reaction energies of 3d transition metal oxides using a hierarchy of exchange-correlation functionals, Phys. Rev. B 88 (2013) 245204.

[24] P.E. Blöchl, Projector augmented-wave method, Phys. Rev. B 50 (1994) 17953–17979.

[25] S. Grimme, J. Antony, S. Ehrlich, H. Krieg, A consistent and accurate ab initio parametrization of density functional dispersion correction (DFT-D) for the 94 elements H-Pu, J. Chem. Phys. 132 (2010) 154104–154122.

[26] V.I. Anisimov, F. Aryasetiawan, A.I. Lichtenstein, First-principles calculations of the electronic structure and spectra of strongly correlated systems: the LDA + U method, J. Phys. Condens. Matter 9 (1997) 767–808.

[27] S.L. Dudarev, G.A. Botton, S.Y. Savrasov, C.J. Humphreys, A.P. Sutton, Electron-energy-loss spectra and the structural stability of nickel oxide: An LSDA+U study, Phys. Rev. B 57 (1998) 1505–1509.

[28] S.M.O. Souvi, M. Badawi, J.-F. Paul, S. Cristol, L. Cantrel, A DFT study of the hematite surface state in the presence of H_2, H_2O and O_2, Surf. Sci. 610 (2013) 7–15.

[29] A. Rohrbach, J. Hafner, G. Kresse, Ab initio study of the (0001) surfaces of hematite and chromia: Influence of strong electronic correlations, Phys. Rev. B 70 (2004) 125426–125443.

[30] H.J. Monkhorst, J.D. Pack, Special points for Brillouin-zone integrations, Phys. Rev. B 13 (1976) 5188–5192.

[31] S. Baroni, S. de Gironcoli, A. Dal Corso, P. Giannozzi, Phonons and related crystal properties from density-functional perturbation theory, Rev. Mod. Phys. 73 (2001) 515–562.

[32] M. Gajdoš, K. Hummer, G. Kresse, J. Furthmüller, F. Bechstedt, Linear optical properties in the projector-augmented wave methodology, Phys. Rev. B 73 (2006) 45112.

[33] R.F.W. Bader, Atoms in Molecules. A Quantum Theory, Oxford University Press (1990).

[34] G. Henkelman, A. Arnaldsson, H. Jónsson, A fast and robust algorithm for Bader decomposition of charge density, Comput. Mater. Sci. 36 (2006) 354–360.

[35] B. Diawara, ModelView, www.modelview.fr/.

[36] D. Costa, K. Sharkas, M.M. Islam, P. Marcus, Ab initio study of the chemical states of water on $Cr_2O_3(0001)$, Surf. Sci. 603 (2009) 2484–2493.

[37] A. Rohrbach, J. Hafner, G. Kresse, Ab initio study of the (0001) surfaces of hematite and chromia: Influence of strong electronic correlations, Phys. Rev. B 70 (2004) 125426–125443.

[38] L.W. Finger, R.M. Hazen, Crystal structure and isothermal compression of Fe_2O_3, Cr_2O_3, and V_2O_3 to 50 kbars, J. Appl. Phys. 51 (1980) 307–313.

[39] N.J. Mosey, E.A. Carter, Ab initio LDA+U prediction of the tensile properties of chromia across multiple length scales, J. Mech. Phys. Solids 57 (2009) 287–304.

[40] S. Funk, T. Nurkic, B. Hokkanen, U. Burghaus, CO_2 adsorption on Cr(110) and $Cr_2O_3(0001)$/Cr(110), Appl. Surf. Sci. 253 (2007) 7108–7114.